Ecological and environmental stability in offshore Southern California Marine Basins through the Holocene

Hannah M. Palmer[1,2], Tessa M. Hill[1,2], Esther G. Kennedy[1,2], Peter Roopnarine[3], Sonali Langlois[4], Katherine R. Reyes[5], and Lowell Stott[6]

1. Earth and Planetary Sciences, University of California, Davis
2. Bodega Marine Laboratory, University of California, Davis
3. California Academy of Sciences
4. Santa Rosa Junior College
5. Dominican University of California
6. University of Southern California

Contents of this file

Introduction

Supporting information contains five supporting figures and two supporting tables. All methodology is discussed in main text.
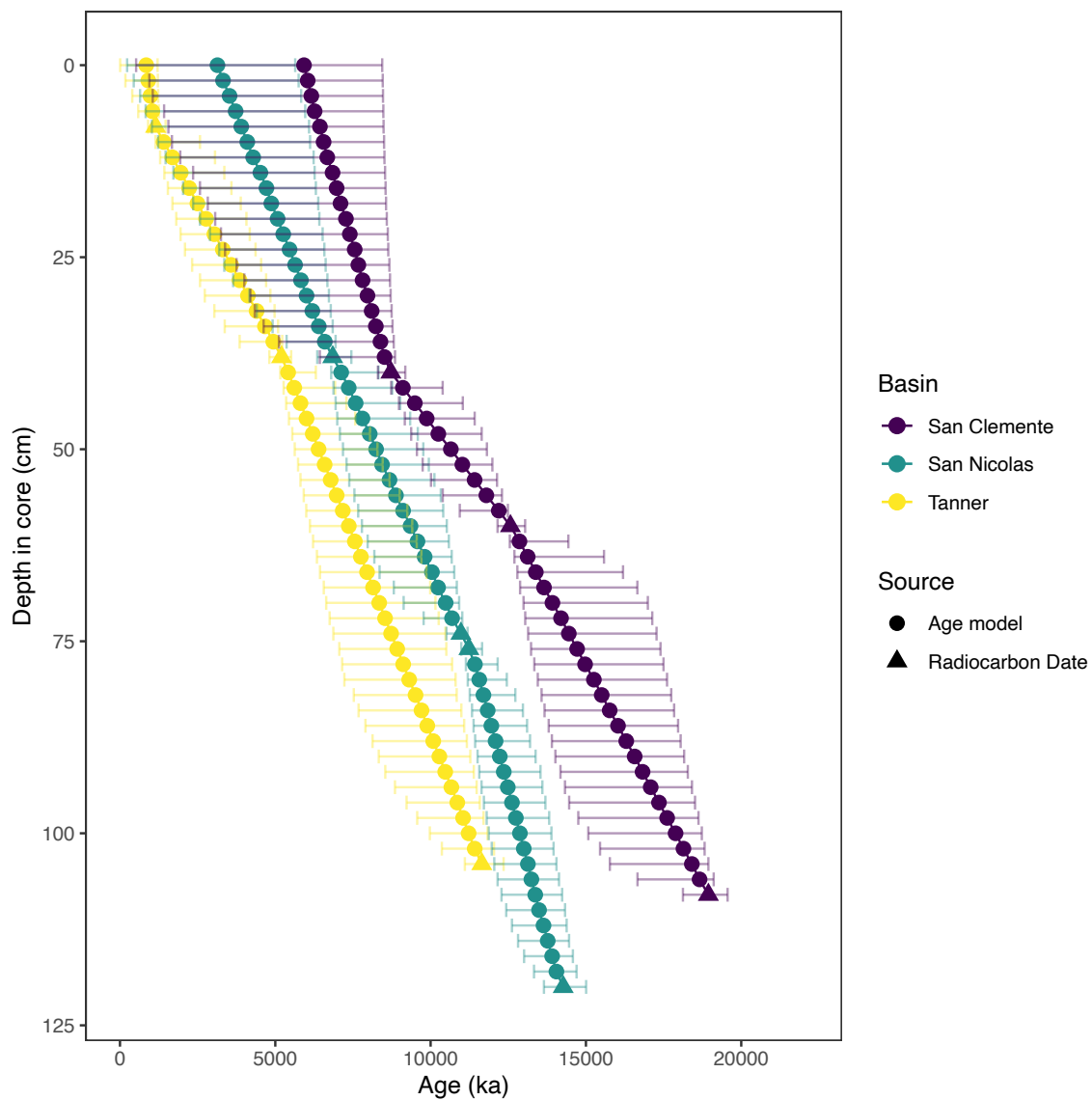
Figure S1. Radiocarbon-based age model as generated through Bchron for three cores included in study. Age shown in thousands of years before present. Triangles are calibrated radiocarbon ages, circles are median ages generated through Bchron age model: Tanner= yellow, San Nicolas = green, San Clemente = purple). Error bars indicate 95% credible interval at each depth.
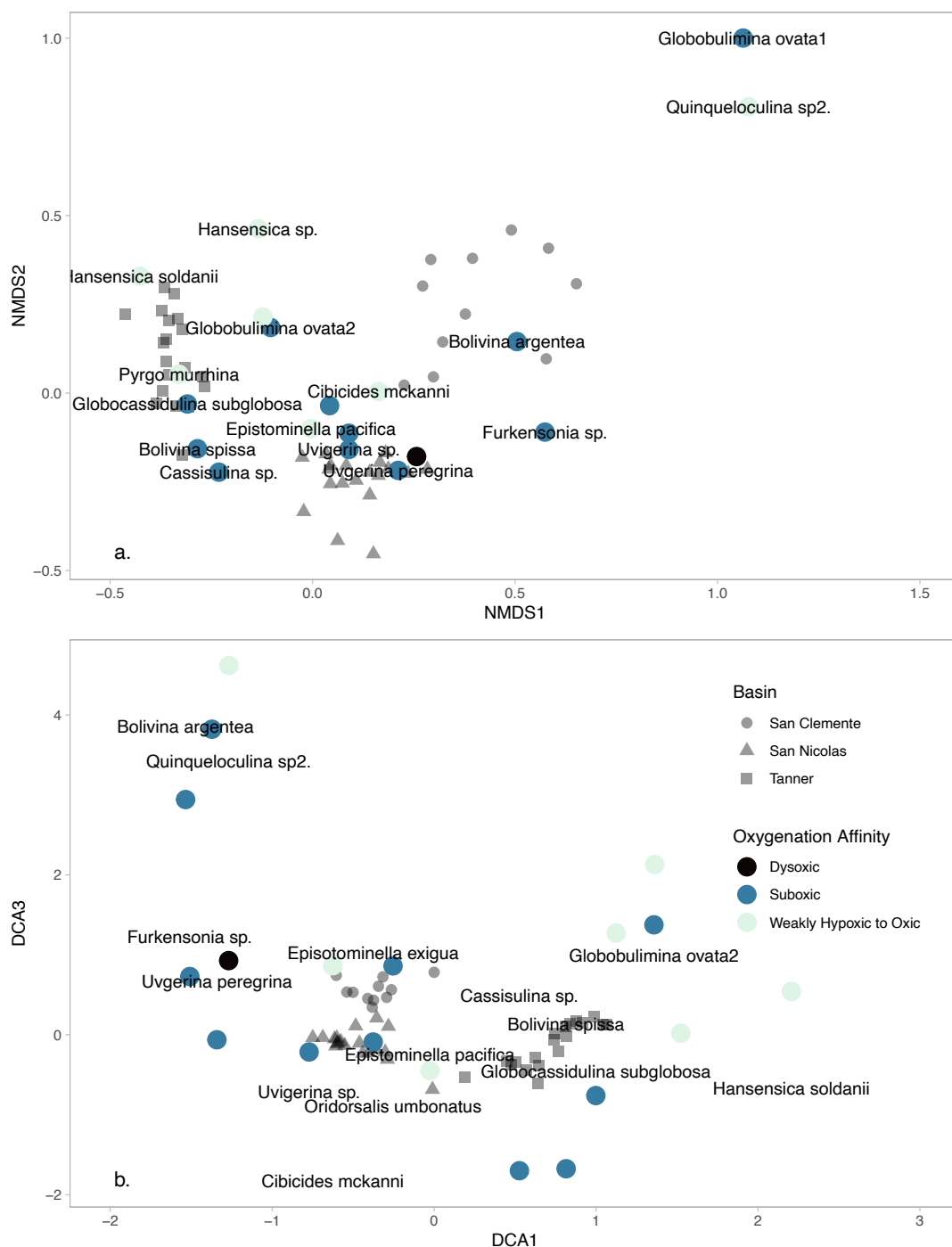
Figure S2. Non-metric multidimensional scaling plot (a.) and detrended correspondence plot (b.) of all benthic foraminiferal assemblages through time from three cores. Axes that represent the most variance are shown here. Species are large circles color coded by published oxygenation affinity (dark blue is dysoxic, blue is suboxic, and teal gray is weakly hypoxic to oxic). All other points represent assemblages at each interval through time at each of the three cores; gray dots are San Clemente assemblage, gray triangles are San Nicolas assemblage, and gray squares are Tann assemblage.
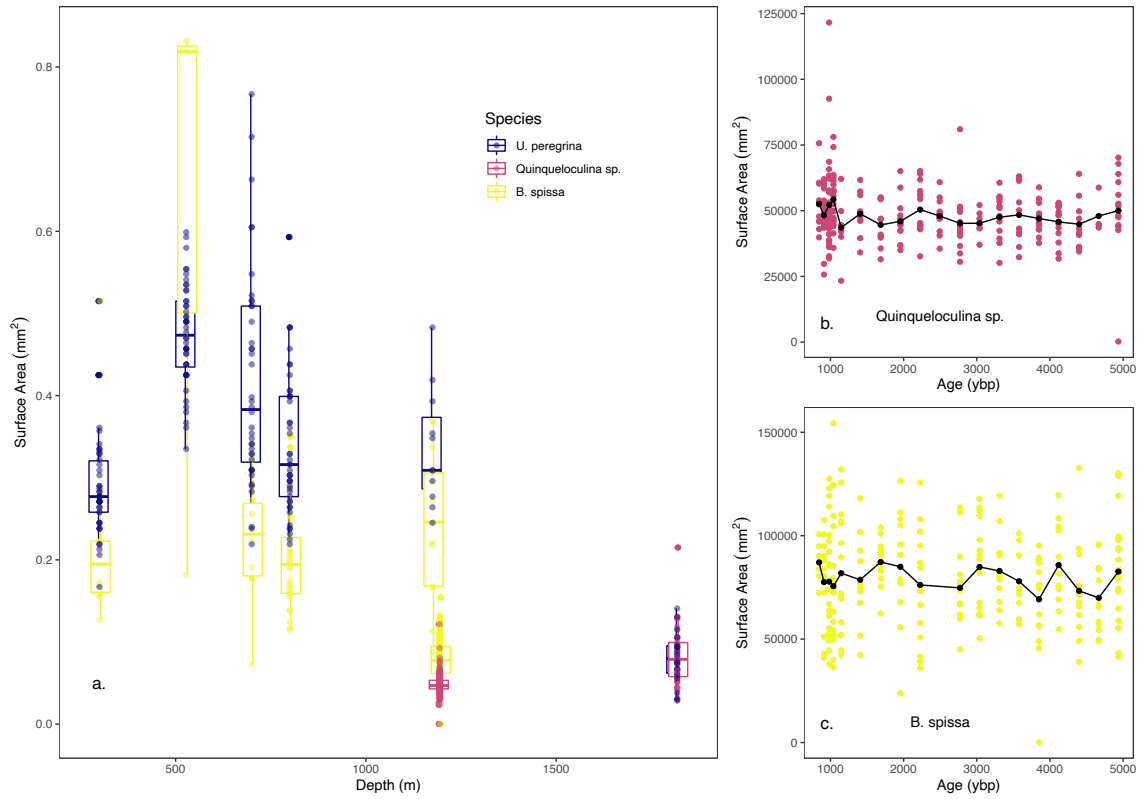
Figure S3. Shell surface area (mm^2) vs. water depth (m) at all points in time (a.). Data shown here indicate all points in time from each water depth. Colors represent species: U. peregrina = purple, *Quinqueloculina* sp. = magenta*, B. spissa* = yellow. All points are shown in addition to box plot. Box plot is slightly offset to better display two species at each water depth. Surface area of *Quinqueloculina* sp. (b.) and *B. spissa* (c.) vs. time in years before present from Tanner Basin.
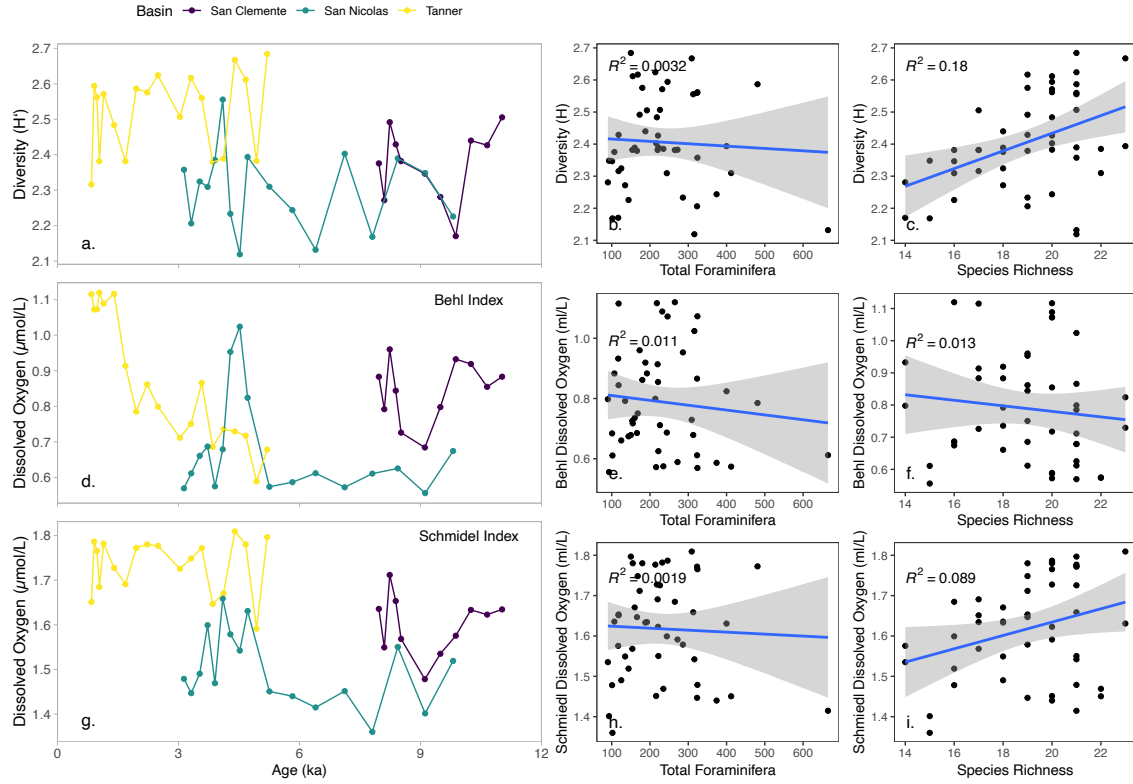
Figure S4. Diversity (Shannon Index), vs. age in thousands of years before present (a.), total foraminifera (b.), and species richness (c.). Reconstructed dissolved oxygen (ml/L) using Behl Index vs. age in thousands of years before present (a.), total foraminifera (b.), and species richness (c.). Reconstructed dissolved oxygen (ml/L) using Schmiedl Index vs. age in thousands of years before present (a.), total foraminifera (b.), and species richness (c.). Trendlines in panels b., c., e., f., h., and i., use linear regression, R^2 is shown on plot.
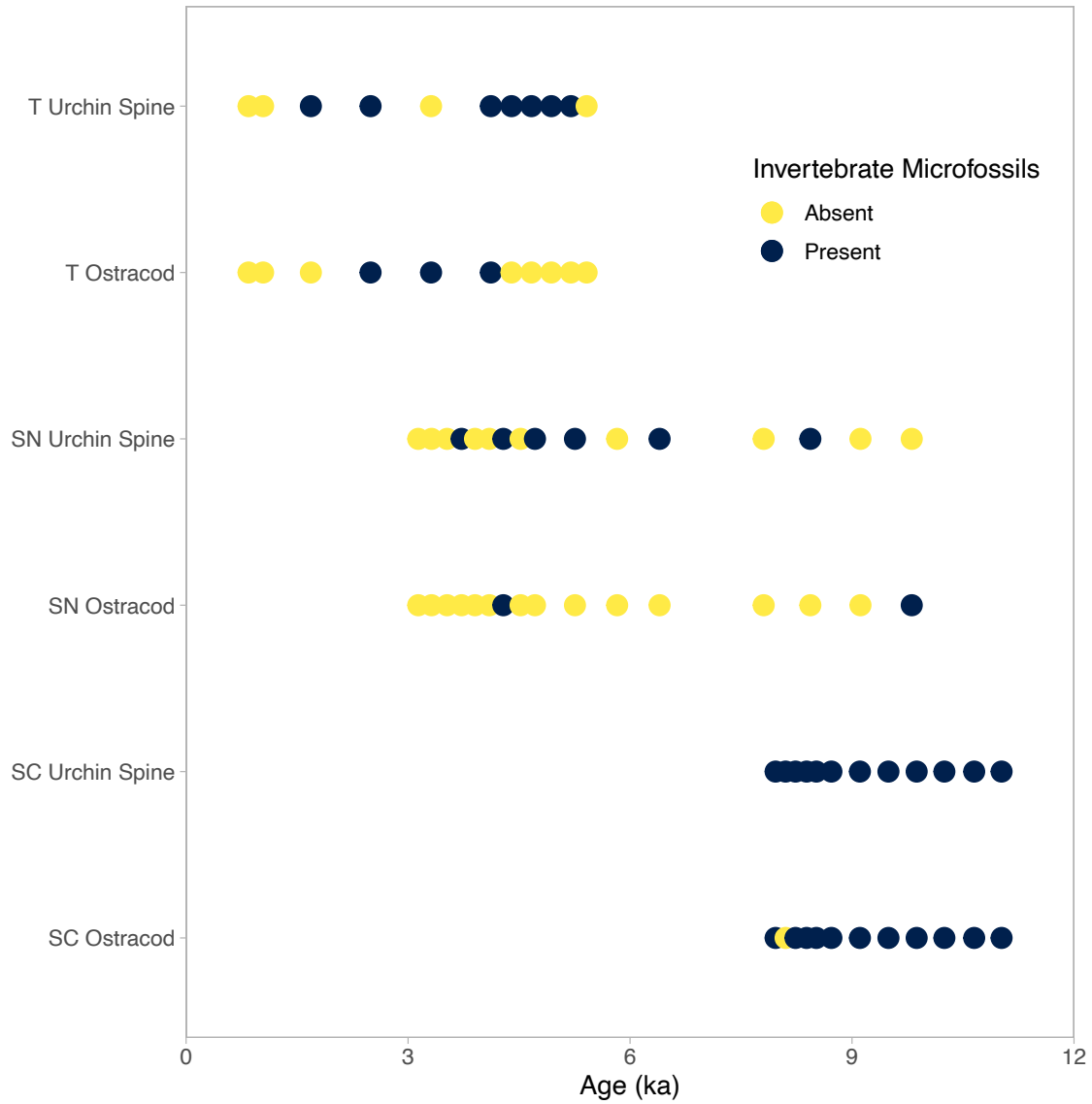
Figure S5: Presence and absence of metazoan microfossils (urchin spines and ostracods) through time (age in thousands of years before present) for each basin (Tanner (T), San Nicolas (SN), and San Clemente (SC)). Presence is blue, absence is yellow.

Basin	Core	Sample Interval	Source	Radiocarbon date (14C years)	±	Calendar age (years before present)	95% Credible Interval (years before present)
Tanner	EW95 04-09	8-10 cm	Stott et al., 2000	1950	50	1146	905-1468
Tanner	EW95 04-09	38- 40 cm	This paper	5290	30	5201	4809-5511
Tanner	EW95 05-09	104-106 cm	Stott et al., 2000	10790	60	11647	11102-12350
San Nicolas	EW95 04-08	38-40 cm	Stott et al., 2000	6780	50	6849	6351-7448
San Nicolas	EW95 04-08	74-76 cm	This paper	10330	35	10976	10511-11190
San Nicolas	EW95 04-08	76-78 cm	Stott et al., 2000	10460	70	11233	10987-11657
San Nicolas	EW95 04-08	120-122 cm	Stott et al., 2000	12870	160	14269	13647-15006
San Clemente	EW95 04-08	40-42 cm	Stott et al., 2000	8550	60	8721	8308-9185
San Clemente	EW95 04-08	60-62 cm	This paper	11430	40	12570	12155-13043
San Clemente	EW95 04-08	108-110 cm	Stott et al., 2000	16650	50	18942	181123-19560

Table S1. Radiocarbon ages and age model for all three cores examined here. Radiocarbon age calibrated using reservoir age of 220 +- 40 and Bchron Bayesian approach.

Species	Oxygen Classification	Modified from Sharon-Behl	Citation for oxygenation affinity
Bolivina argentea	Suboxic		Sharon et al., 2021
Bolivina pseudobeyrichi	Dysoxic		Sharon et al., 2021
Bolivina spissa	Suboxic		Sharon et al., 2021
Bulimina tenuata	Dysoxic		Sharon et al., 2021
Cassidulina sp.	Suboxic		Sharon et al., 2021
Chlistomella ovoidea	Suboxic		Sharon et al., 2021
Cibicides mckannai	Weakly hypoxic to oxic	Modified	Kaiho 1994
Cibicides sp.	Weakly hypoxic to oxic	Modified	Kaiho 1994
Elphidium sp.	Weakly hypoxic to oxic		Sharon et al., 2021
Epistominella exigua	Suboxic		Sharon et al., 2021
Epistominella pacifica	Weakly hypoxic to oxic	Modified	Cannariato and Kennett 1999
Fursenkoina sp.	Suboxic	Modified	Kaiho 1994
Globobulimina barbata	Suboxic	Modified	Ohkushi et al., 2013
Globobulimina ovata1	Suboxic	Modified	Ohkushi et al., 2013
Globobulimina ovata2	Suboxic	Modified	Ohkushi et al., 2013
Globobulimina pacifica	Suboxic	Modified	Ohkushi et al., 2013
Globocassidulina sp.	Suboxic		Sharon et al., 2021
Globocassidulina subglobosa	Suboxic		Sharon et al., 2021
Hanzeniisca soldanii	Weakly hypoxic to oxic	Modified	De and Gupta 2010
Hanzeniisca sp.	Weakly hypoxic to oxic	Modified	De and Gupta 2010
Melonis affinis	Suboxic	Modified	Kaiho 1994
Nonionella stella	Dysoxic		Sharon et al., 2021
Oridorsalis umbonatus	Suboxic		Sharon et al., 2021
Other			
Pyrgo murrhina	Weakly hypoxic to oxic		Sharon et al., 2021
Quinqueloculina sp.	Weakly hypoxic to oxic		Sharon et al., 2021
Quinqueloculina sp2.	Weakly hypoxic to oxic		Sharon et al., 2021
Uvigerina peregrina	Suboxic		Sharon et al., 2021
Uvigerina proboscoidea	Suboxic		Sharon et al., 2021
Uvigerina sp.	Suboxic		Sharon et al., 2021

Table S2. Oxygen affinity for all species examined here and utilized in oxygen transfer functions.

	NMDS1 (43.0%)	NMDS2 (15.8%)	NMDS3 (3.1%)	NMDS4 (0.8%)
Bolivina spissa	-0.284	-0.157	0.167	-0.042
Cassisulina sp.	-0.232	-0.223	0.080	-0.085
Cibicides mckanni	0.163	0.005	-0.153	0.166
Epistominella pacifica	-0.004	-0.100	-0.046	0.122
Episotominella exigua	0.089	-0.113	-0.040	-0.059
Globobulimina ovata2	-0.104	0.185	0.005	-0.089
Globocassidulina subglobosa	-0.309	-0.031	0.045	0.033
Hansensica soldanii	-0.427	0.329	-0.075	0.076
Oridorsalis umbonatus	0.042	-0.035	-0.123	0.103
Pyrgo murrhina	-0.330	0.053	-0.007	0.049
Quinqeloculina sp.	-0.123	0.214	0.101	-0.041
Uvigerina sp.	0.090	-0.159	-0.068	0.038
Uvgerina peregrina	0.211	-0.218	-0.028	0.004
Hansensica sp.	-0.135	0.463	-0.357	-0.239
Nonionella stella	0.257	-0.179	-0.072	-0.141
Bolivina argentea	0.505	0.145	-0.813	-0.953
Furkensonia sp.	0.574	-0.110	0.239	0.125
Quinqeloculina sp2.	1.077	0.806	0.276	-0.216
Globobulimina ovata1	1.063	1.000	0.611	0.317

Table S3. NMDS species scores. Proportion of variance for each axis is reported in parenthetical. Proportion of variance of each axis was calculated summarized by each axis using the Pearson correlation between the Euclidean dissimilarity of the sites scores and the Bray-Curtis dissimilarity of the faunal abundances for each site with the mantel function in the "ecodist" package (Sharon et al., 2021).

	DCA1 (45.6%)	DCA2 (6.2%)	DCA3 (11.3%)	DCA4 (2.1%)
Bolivina spissa	0.815	0.132	-1.676	-0.235
Cassisulina sp.	0.527	0.490	-1.701	-0.720
Cibicides mckanni	-0.626	-1.833	0.864	0.333
Epistominella pacifica	-0.026	-0.248	-0.447	1.073
Episotominella exigua	-0.376	1.024	-0.091	-1.480
Globobulimina ovata2	1.358	0.997	1.375	-1.259
Globocassidulina subglobosa	0.999	-0.456	-0.761	-0.038
Hansensica soldanii	2.207	-0.665	0.544	0.706
Oridorsalis umbonatus	-0.253	-0.897	0.861	-0.859
Pyrgo murrhina	1.523	-0.763	0.020	0.498
Quinqeloculina sp.	1.124	0.525	1.273	1.365
Uvigerina sp.	-0.772	-0.713	-0.215	0.231
Uvgerina peregrina	-1.341	0.669	-0.063	0.199
Hansensica sp.	1.362	-0.780	2.129	-2.557
Nonionella stella	-1.269	1.092	0.928	0.723
Bolivina argentea	-1.535	3.864	2.943	1.728
Furkensonia sp.	-1.508	1.231	0.729	1.057
Quinqeloculina sp2.	-1.267	3.421	4.619	2.955
Globobulimina ovata1	-1.372	3.262	3.822	4.412

Table S4. DCA species scores. Proportion of variance for each DCA axis is reported in parenthetical. Proportion of variance of each axis was calculated summarized by each axis using the Pearson correlation between the Euclidean dissimilarity of the DCA sites scores and the Bray-Curtis dissimilarity of the faunal abundances for each site with the mantel function in the "ecodist" package (Sharon et al., 2021).